Available online at www.sciencedirect.com

SciVerse ScienceDirect

Journal of the European Ceramic Society 32 (2012) 915–923

www.elsevier.com/locate/jeurceramsoc

Preparation and characterization of reticular SSC cathode films by electrostatic spray deposition

C.L. Chang [a,b], T.F. Chu [c], C.S. Hsu [d], B.H. Hwang [a,*]

[a] Department of Materials Science and Optoelectronics Engineering, National Sun Yat-Sen University, Kaohsiung 80424, Taiwan
[b] Institute of Nuclear Energy Research, Atomic Energy Council, Taoyuan 32546, Taiwan
[c] Department of Materials Science and Engineering, National Formosa University, Huwei Township, Yunlin County 632, Taiwan
[d] Kaohsiung Municipal Chung-Cheng Industrial High School, Kaohsiung 80656, Taiwan

Received 1 June 2011; received in revised form 1 October 2011; accepted 3 November 2011
Available online 23 November 2011

Abstract

$Sm_{0.5}Sr_{0.5}CoO_{3-\delta}$ (SSC) cathode films were deposited on CGO ($Gd_{0.1}Ce_{0.9}O_{1.95}$) electrolyte substrates by electrostatic spray deposition to prepare SSC/CGO/SSC symmetrical cells. Deposition parameters were changed systematically to examine their effects on film microstructure and electrode performance. A set of deposition parameters including a 0.01 M precursor solution containing metal nitrates in a mixture solvent of de-ionized water (0.6 vol%), ethanol (1.5 vol%) and diethyl butyl carbitol (97.9 vol%), a flow rate of 6 ml/h for precursor solution, a deposition temperature of 350 °C and an imposed electric field of 10 kV/3 cm was identified for preparation of films with a highly porous reticular structure. The superior performance of a reticular SSC electrode was evidenced by its low interfacial resistances of 0.275 and 0.018 $\Omega\,cm^2$ measured in 500 and 700 °C, respectively. These values were one-half to one order of magnitude smaller than that of the screen-printed or slurry-painted electrodes.

Keywords: $Sm_{0.5}Sr_{0.5}CoO_{3-\delta}$; Electrostatic spray deposition; Impedance; Reticular structure; Solid oxide fuel cell

1. Introduction

Electrostatic spray deposition (ESD) is a spray pyrolysis method for solid film deposition[1–7] where the aerosol droplets are generated by an electrostatic field. This technique has several advantages over conventional deposition techniques, such as a simple and cost-effective set-up, inexpensive and non-toxic precursors, atomic-scale mixing of precursor elements, easy doping even with multiple elements, high deposition efficiency, direct deposition under ambient atmosphere and easy control of surface morphology of the deposited films. Because the porosity of deposited films can be easily controlled by adjusting the deposition parameters such as temperature, applied electrostatic field strength and flow rate and concentration of the precursor solution, ESD is particularly suitable for deposition of electrode films for solid oxide fuel cells (SOFC) where high porosity is required for diffusion of fuel and air/oxygen gases. Although ESD has been used to deposit films of various electrode materials,[8–18] these studies concentrated on the microstructure investigation of deposited films and no electrochemical test was carried out to evaluate the effects of changing deposition parameters and film morphology.

Among the various morphologies of SOFC electrodes obtained by ESD, a unique reticular structure of high porosity was reported by Princivalle et al. in La(Sr)$MnO_{3-\delta}$ (LSM) and LSM/YSZ ($Y_{0.08}Zr_{0.92}O_x$) cathode[16–18] and by Taniguchi and Hosokawa in NiO-SDC ($Sm_{0.2}Ce_{0.8}O_x$) anode[10] films. Electrode films of this reticular structure possessed high porosity and high surface area and hence were expected to exhibit good electrochemical performance. Recently, $Sm_{0.5}Sr_{0.5}CoO_{3-\delta}$ (SSC) cathode with this reticular structure was deposited to obtain an SSC/$BaZr_{0.1}Ce_{0.7}Y_{0.2}O_{3-\delta}$ (BZCY)/NiO-BZCY single cell in our laboratory and a peak power of 863 mW cm^{-2} at 700 °C was obtained in the subsequent test.[19] Although the overall performance of the single cell was revealed by the peak power, the

* Corresponding author. Tel.: +886 7 5252000x4059; fax: +886 7 5254099.
E-mail address: zorro@mail.nsysu.edu.tw (B.H. Hwang).

0955-2219/$ – see front matter © 2011 Elsevier Ltd. All rights reserved.
doi:10.1016/j.jeurceramsoc.2011.11.001

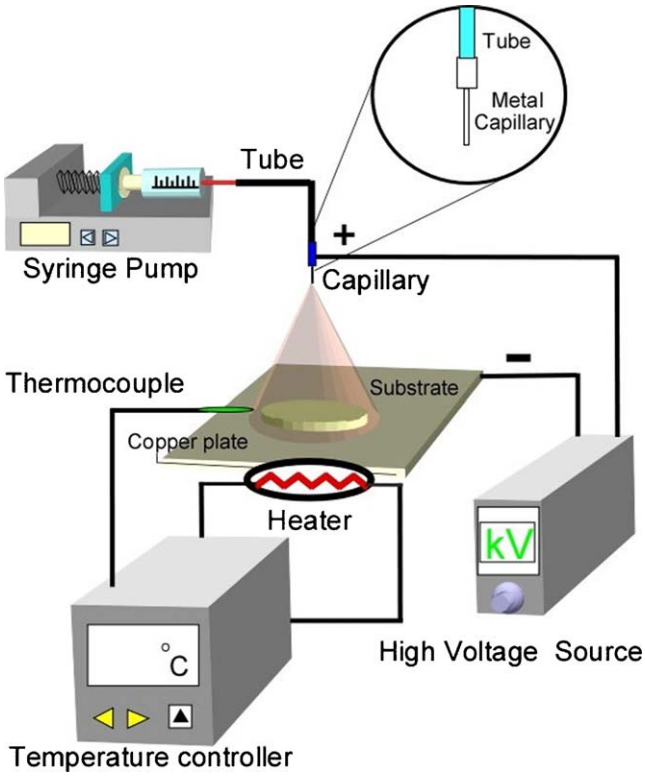

Fig. 1. Schematic diagram of the electrostatic deposition setup.

exact performance of the reticular SSC cathode remains to be determined.

In this work, formation and evolution of reticular stucture of SSC electrodes were investigated. The corresponding electrochemical performance was also evaluated by AC impedance measurement and compared with that of screen-printed and slurry-painted SSC electrodes.

2. Experimental

2.1. Preparation of SSC/CGO ($Gd_{0.1}Ce_{0.9}O_{1.95}$)/SSC symmetrical cells

The precursor solution for ESD was prepared by dissolving 0.001 mol $Sm(NO_3)_3{\cdot}6H_2O$ (Strem, 99.9%), 0.001 mol $Sr(NO_3)_2$ (Showa, 98%) and 0.002 mol $Co(NO_3)_2{\cdot}6H_2O$ (Aldrich, 98%) in a mixture solvent of de-ionized water (0.6 vol%), ethanol (1.5 vol%) and 2-(2-butoxyethoxy)-ethanol (butyl carbitol, $C_8H_{18}O_3$, 97.9 vol%), the total concentration of metal ions was 0.01 M.

As shown in the schematic diagram of Fig. 1, the precursor solution was pumped by a syringe pump (KDS, KD-100) to the tip of a stainless steel capillary (Terumo, No. 17) where it was atomized by the electrostatic field (Acopian, PH030HA1) imposed between the capillary and a copper plate on which the CGO disk substrate sat. The capillary-substrate distance and flow rate of the precursor solution were kept at 3 cm and 6 ml/h, respectively throughout this work. The capillary was scanned over the substrate via an *x–y* table at a speed of 3 mm/s, and the substrate was heated by a heater beneath the copper plate and kept at a fixed temperature by the connected thermal couple and temperature controller during the deposition process. The CGO disks of 15 mm diameter and 0.5 mm thickness were prepared by solid state sintering (1400 °C for 4 h) green compacts of CGO powder (Rhodia GDC 91-SY). Post-deposition calcination at 800 °C for 2 h was carried out to promote crystallization. The heating and cooling rates before and after the calcination were 2.5 °C/min and 3.2 °C/min, respectively.

SSC electrodes were prepared on both sides of the CGO disks by ESD method to obtain symmetrical cells for subsequent microstructure examination and electrochemical performance evaluation. Deposition parameters were systematically changed to identify the parameter values required for deposition of SSC reticular films. Evolution and formation of the reticular structure was further studied by examining films obtained with successively increasing deposition times using the identified deposition parameters.

Similar symmetrical cells were also prepared by screen-printing SSC slurry on both sides of CGO disks for comparison. The slurry was prepared by dissolving 1 g SSC powder and 1 g ethyl cellulose (as binder) into 10 ml α-terpineol followed by thorough stirring and mixing. The SSC powder was prepared by a glycine-nitrate method. $Sm(NO_3)_3{\cdot}6H_2O$, $Sr(NO_3)_2$, $Co(NO_3)_2{\cdot}6H_2O$ and glycine (CH_2NH_2COOH) in mole ratio of 0.5:0.5:1.0:4 were dissolved in de-ionized water to obtain a precursor solution with a concentration of 0.4 M for total metal ions. After complete mixing, the solution was baked in 100 °C till a viscous gel was formed and then heated to 300 °C to ignite combustion. SSC raw powder obtained after combustion was calcined in 950 °C for 5 h to obtain crystalline powders.

2.2. Characterization

In order to understand the pyrolysis process in detail, simultaneous thermogravimetric analysis (TGA) and differential thermal analysis (DTA) measurement was carried out (Seiko SSC 5000) for the precursor solution. The precursor solution was baked to obtain a nearly dry sample of 8.034 mg before the TGA and DTA measurement. The measurement was performed in the temperature of 25–900 °C in nitrogen with a heating rate of 10 °C/min.

Phase identification was carried out for the deposited cathodes using an X-ray powder diffractometer (Siemens D5000) with a Cu tube and a quartz monochromator on the diffracted beam side. A scanning electron microscope (SEM, Joel, JSM-6330) was used for observation of their morphologies. AC impedances of symmetrical cells were measured using a potentiostat/galvanostat (Autolab PGSTAT30) with an excitation voltage amplitude of 10 mV. The impedance spectra were recorded over the frequency range of 0.01–100 kHz in the temperature of 500–700 °C under ambient air and open circuit condition. Interfacial area specific resistances (ASR) of the SSC cathodes in contact with the CGO electrolyte were extracted from the impedance spectra. The variation of ASRs with the SSC cathode morphology was examined. The

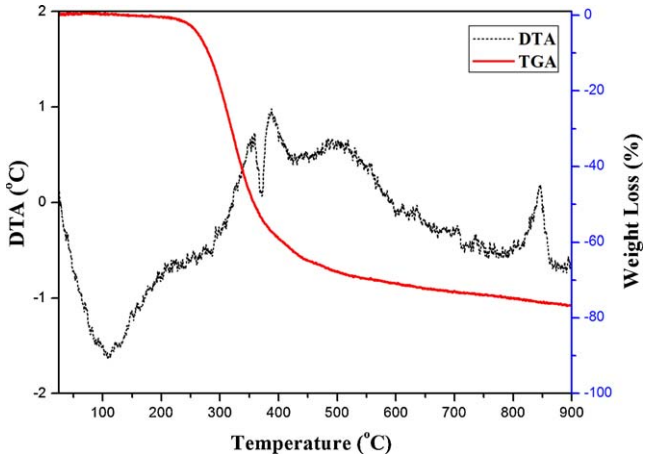

Fig. 2. TGA/DTA curves of the nearly dry SSC precursor.

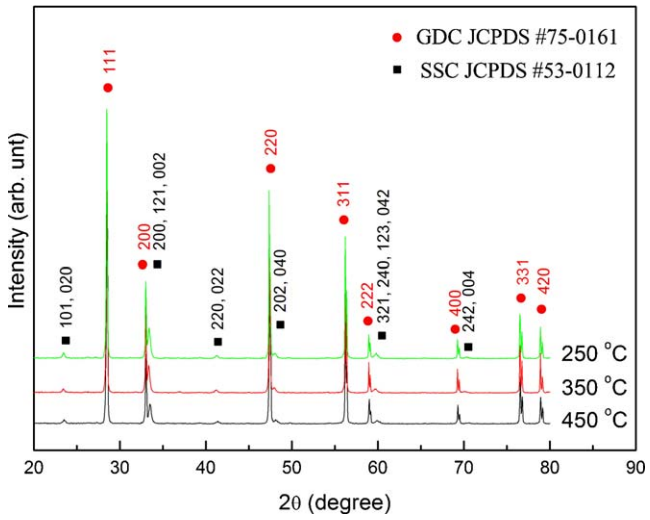

Fig. 3. XRD patterns of SSC cathode films obtained at different deposition temperatures.

ASR values of reticular SSC cathode prepared by ESD were compared with that prepared by screen-printing and slurry-painting.

3. Results and discussion

The TGA curve in Fig. 2 shows an initial slow weight loss of about 3% before 250 °C followed by a rapid loss of ~67% between 250 °C and 550 °C and another slow loss of ~6% between 550 °C and 900 °C. The initial weight loss is attributed to the evaporation of solvent in the nearly dry sample and the evaporation probably continued beyond 250 °C considering the rapid heating rate of 10 °C/min. The rapid weight loss between 250 and 550 °C can be attributed to the dehydration and decomposition of the nearly dry sample because the calculated weight losses due to dehydration and decomposition of the metal nitrates into oxides of Sm_2O_3, SrO, and Co_2O_3 are 26% and 38% respectively, and their sum (64%) is close to the measured value of 67%. With a 26% weight loss, the dehydration was probably finished around ~320 °C according to the TGA curve. The subsequent decomposition in 320–550 °C was probably a multiple step process because two sharp and one broad exothermic peaks at 358 °C, 385 °C and 498 °C in the DTA curve are observed. The strong exothermic peak at 843 °C in the DTA curve is attributed to the crystallization of the perovskite phase.

To illustrate the effects of deposition parameters on the film microstructure and the subsequent electrochemical performance, the most important deposition parameters, deposition temperature and electric field strength, were changed to prepare two series of samples. The deposition temperature was changed from 250 °C to 350 °C and 450 °C under a fixed electric field strength of 10 kV/3 cm in the temperature series, and the electric field strength was changed from 8 kV/3 cm to 10 kV/3 cm and 12 kV/3 cm under a fixed deposition temperature of 350 °C in the electric field series. The deposition time was 90 min for each sample of these two series. The depositon temperatures of 250, 350 and 450 °C, as shown on the temperature controller, indicated temperatures of the copper heating plate. The corresponding temperatures on the substrate surface, as determined by an infrared temperature gun, were somewhat lower at 210, 266 and 334 °C.

XRD patterns of films of the temperature series are shown in Fig. 3. These XRD patterns are typical for samples prepared in this work and indicate that well crystallized SSC (JCPDS #53-0112) perovskite phase on CGO (JCPDS #75-0161) substrates was obtained after deposition and calcination. The corresponding surface and cross section morphologies are shown in the SEM microphotographs of Fig. 4(a)–(f). Under the low deposition temperature of 250 °C, the temperature on the substrate surface (210 °C) was lower than the boiling point of butyl carbitol (231 °C) and hence aerosol droplets experienced little evaporation before landing on the substrate. The rather wet droplets readily wetted the whole substrate surface to form a continuous, flat film. The as deposited, wet film broke up into separate pieces in post-deposition calcination as the remaining solvent evaporated, the metal nitrates decomposed and the film shrunk. Irregular shaped particles nucleated from the film during calcination (as indicated by arrows in Fig. 4(a)) are also observed. At the deposition temperature of 350 °C (266 °C on the substrate surface), the aerosol droplets experienced considerable evaporation during the flight. With the resultant reduced wetting and spreading on the substrate, each aerosol droplet formed only a small layer after landing. Moreover, isolated holes were developed in the small layer during the quick drying and spreading of the aerosol droplet. Connection and overlapping of these holey layers proceeded with deposition to form a reticular film as shown in Fig. 4(c) and (d). More detailed formation and growth sequences of this reticular structure will be further addressed later. When the deposition temperature was raised to 450 °C (334 °C on the substrate surface), the landing aerosol droplets were so dry that they solidified rapidly to form isolated particles sticking to their landing positions after the very limited wetting. Assembly of these dried particles resulted in a rather rough film as shown in Fig. 4(e) and (f) where isolated particles formed in the final deposition stage were found scattering on the film surface.

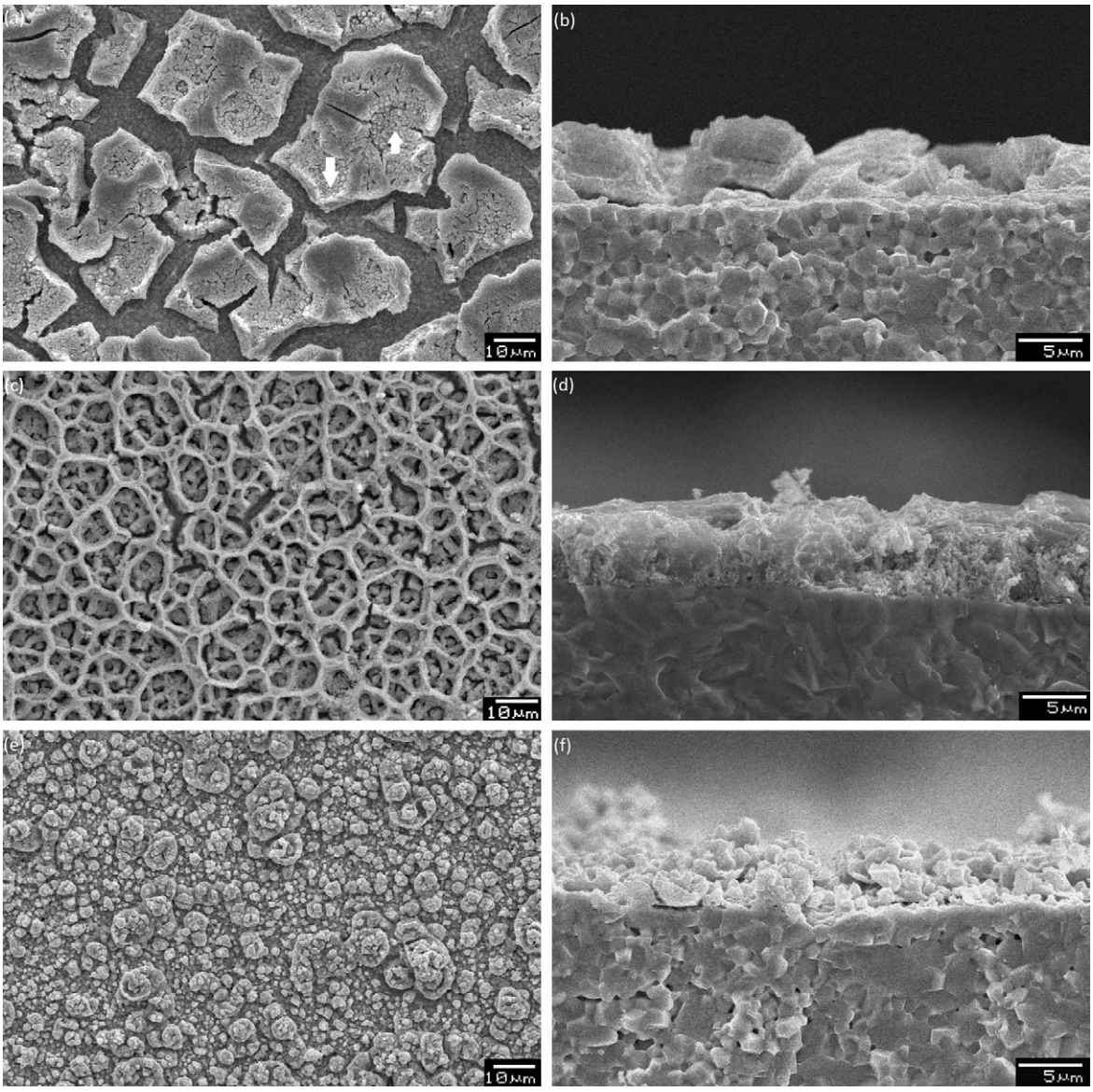

Fig. 4. SEM micrographs of calcined SSC films prepared at a deposition temperature of (a and b) 250 °C; (c and d) 350 °C; and (e and f) 450 °C.

The impedance spectra obtained under different operation temperatures for the symmetrical cell prepared at a deposition temperature of 350 °C are shown in Fig. 5(a), while that obtained under the operation temperature of 600 °C for cells prepared with different deposition temperatures are shown in Fig. 5(b). Each impedance arc intercepts the Z' axis at two ends, and the difference of these two intercepts gives the interfacial ASR of the electrolyte–electrode interface. Note the ohmic resistances of electrolyte and Pt wire beyond the high frequency end were deleted for clarity. Impedance spectra of similar shape were obtained for all cells prepared in this work. The interfacial ASRs of SSC electrodes prepared at different deposition temperatures were extracted from the corresponding impedance spectra and plotted in the Arrhenius plot of Fig. 6. The ASRs of SSC electrode deposited at 350 °C changed from 0.275 Ω cm^2 in the operation temperature of 500 °C, to 0.125, 0.057, 0.024 and 0.018 Ω cm^2, in 550, 600, 650 and 700 °C, respectively. These values were smaller than that deposited at 250 °C or 450 °C by two orders of magnitude. The superior performance of the 350 °C-deposited SSC electrode was apparently due to the high porosity and high surface area and hence high population of reaction sites inherent in its reticular structure. In contrast, SSC electrodes deposited at 250 °C and 450 °C, lacking the open structure of a reticular film, possessed much less sites for oxygen reduction reaction.

Surface and cross section morphologies of electric field series electrodes are shown in Fig. 7(a)–(f). Comparing to the electrode deposited in 10 kV/3 cm (Fig. 7(c) and (d)), electrodes deposited in 8 kV/3 cm and 12 kV/3 cm are denser and less promising for cathode performance. In the relatively low electric field of 8 kV/3 cm, the electrostatic force was weaker resulting in less spreading of the aerosol jet and coarser aerosol droplets. In fact,

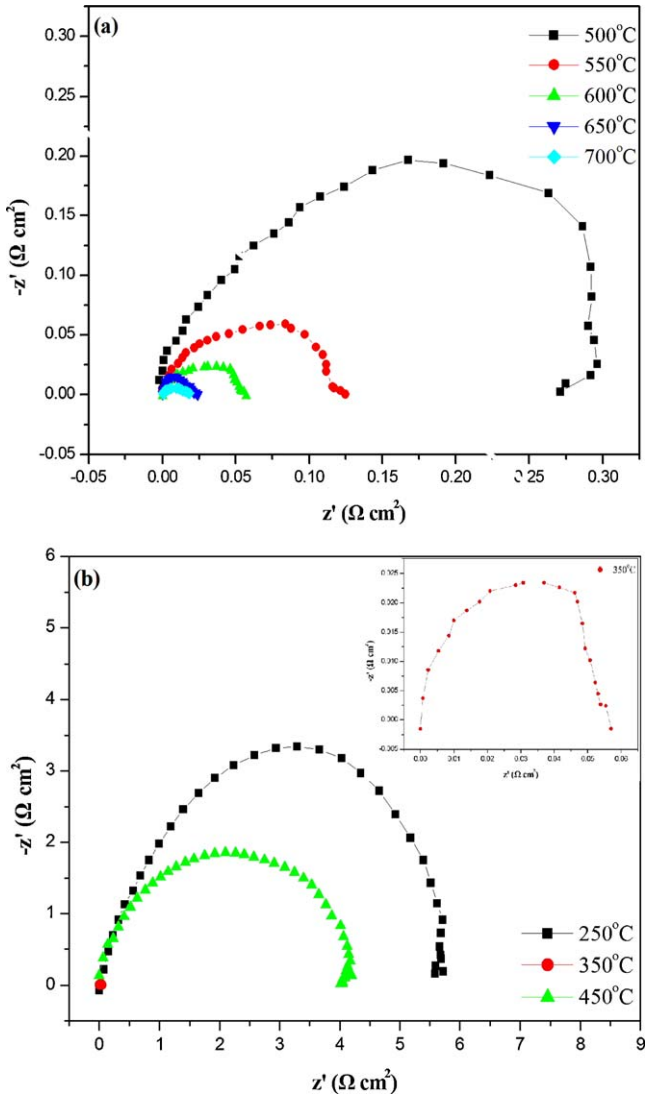

Fig. 5. Impedance spectra of (a) the 350 °C-deposited symmetrical cell measured in 500–700 °C, (b) symmetrical cells prepared at deposition temperatures of 250, 350 and 450 °C measured in 600 °C.

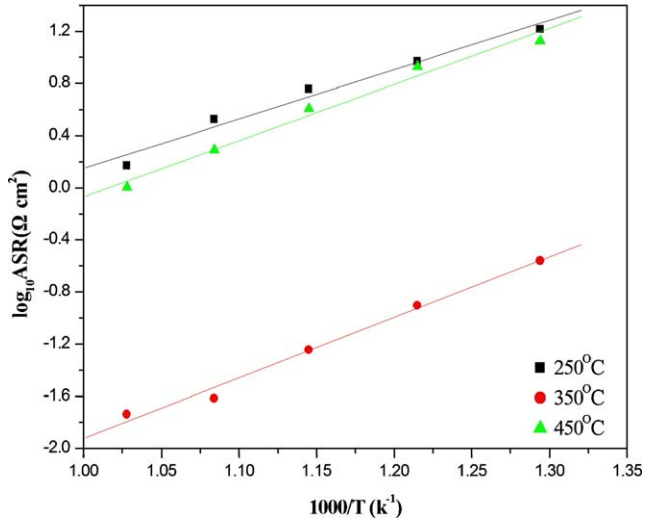

Fig. 6. Arrhenius plots of interfacial ASRs for SSC electrodes prepared at deposition temperatures of 250 °C, 350 °C and 450 °C.

the consequence of a low electric field was even more clearly seen at 6 kV/3 cm where neither atomization nor aerosol jet but dripping was observed (not shown). Although the coarser aerosol droplets were wetter, full wetting of the entire substrate surface was not accomplished and a continuous layer was not formed due to the weak impinging of the aerosol droplets. Each aerosol droplet covered only a small area of a few microns after the limited spreading allowed by the weak impinging, and subsequent solidification resulted in a laminar patch sticking to its original landing position. The abundant solvent remaining in each patch was eliminated in the subsequent drying and calcination leaving plenty pores on the patch surface as shown in Fig. 7(a). When the electric field was increased to 10 kV/3 cm, the increased electrostatic force resulted in stronger impinging and hence more extended spreading of the aerosol droplets. The wetting and spreading were barely enough to allow formation of small holey layers as mentioned above. Connection and overlapping of these holey layers proceeded with deposition to form a reticular film (Fig. 7(c)). When the electric field was increased from 10 kV/3 cm to 12 kV/3 cm, the enhanced electrostatic force resulted in a wide spreading of the aerosol jet and very fine aerosol droplets. The spreading of these fine aerosol droplets via the scanning capillary rendered a more uniform distribution of landing material on the substrate surface. These uniformly distributed aerosol droplets dried and solidified quickly after landing because wetting and spreading were very limited due to their small size. Comparing to that shown in Fig. 7(a), a smoother film was obtained after calcination (Fig. 7(e)) because of the more uniform distribution of the landing material and finer pores were present on the film because of the finer aerosol droplets.

The interfacial ASRs of SSC electrodes prepared at different electric field strengths were extracted from the corresponding impedance spectra (not shown) and shown in the Arrhenius plot of Fig. 8. The SSC electrode prepared at the electric field of 10 kV/3 cm possessed the lowest ASR values as expected due to its high porosity and high surface area. The ASR values of the SSC electrode prepared at the electric field of 12 kV/3 cm were larger than that of the electrode prepared at 8 kV/3 cm because of its denser film structure.

To reveal the formation and growth mechanisms of the reticular structure, a series of SSC films were deposited with increasing deposition durations under 350 °C and 10 kV/3 cm. The morphologies of these films are shown in Fig. 9(a)–(f). After a short deposition time of 1 min (Fig. 9(a)), small thin layers with isolated holes were formed already following the wetting and spreading of aerosol droplets on the substrate after landing. These scattered layers dried out so quickly during their spreading that a complete connection to form a continuous layer covering the whole substrate was not observed at this stage. As the deposition time increased to 2 min, more holes were developed on the initially deposited layers due to the sustained heating from the substrate. Layer thickness increased especially along the rims of holes where drying and solidification happened most readily. As the deposition proceeded, overlapping of these holey layers occurred and the random stacking of the holes in different layers started to form a reticular film as shown in Fig. 9(c) after a deposition time of 5 min. This overlapping and stacking

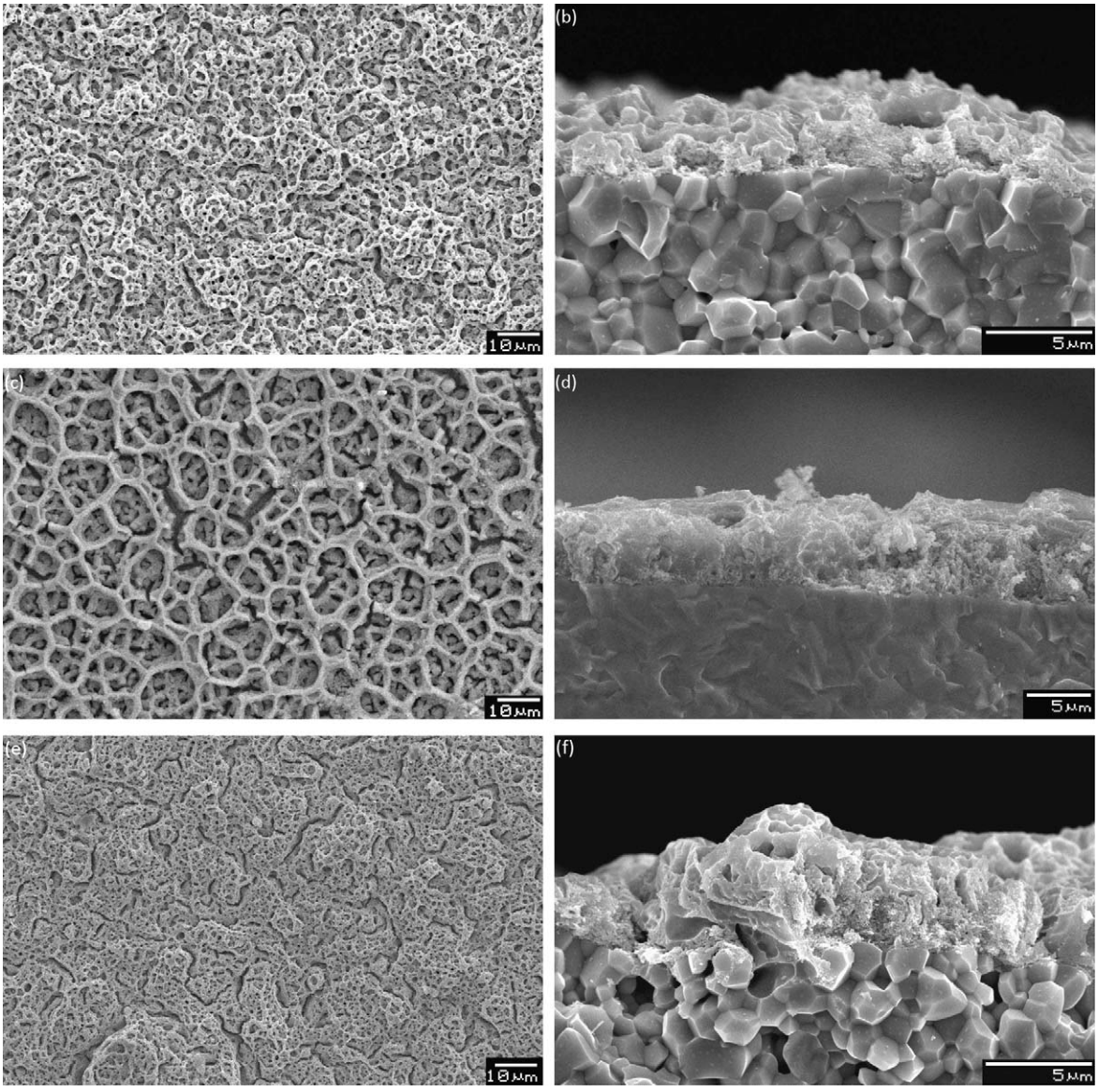

Fig. 7. SEM micrographs of calcined SSC films prepared under a electric field strength of (a and b) 8 kV/3 cm; (c and d) 10 kV/3 cm; (e and f) 12 kV/3 cm.

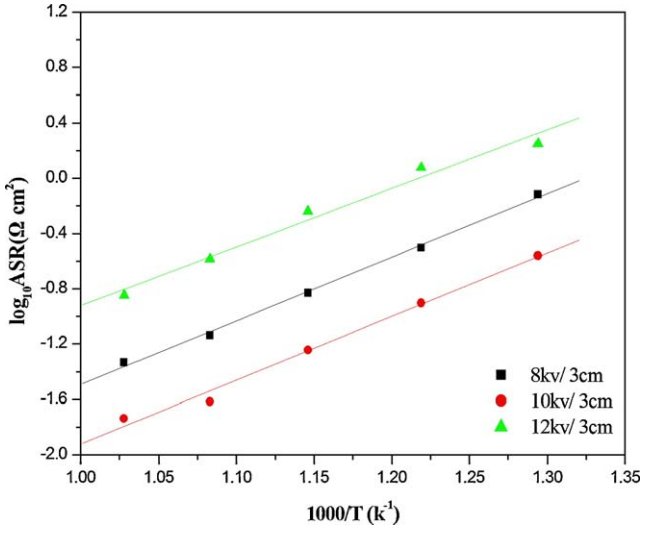

Fig. 8. Arrhenius plots of interfacial ASRs for SSC electrodes prepared at electric field strengths of 8 kV/3 cm, 10 kV/3 cm and 12 kV/3 cm.

process continued to form a complete film covering the whole substrate surface with a well developed reticular structure as shown in Fig. 9(d) after a deposition time of 10 min. Further extending of deposition time resulted in a slight widening of the mesh rims in the reticular structure as shown in Fig. 9(e) and (f) for films obtained in a deposition time of 30 min and 180 min, respectively.

The growth and evolution process shown above indicates that an appropriate wetting and spreading of aerosol droplets on the substrate surface is critical to obtain the reticular structure. The acquisition of the proper wetness in aerosol droplets for the appropriate wetting and spreading requires subtle adjustment of various deposition parameters. In this work, SSC films with a reticular structure were successfully deposited using the following deposition parameters: a 0.01 M precursor solution containing metal nitrates in a mixture solvent of de-ionized water (0.6 vol%), ethanol (1.5 vol%) and 2-(2-butoxyethoxy)-ethanol butyl carbitol (97.9 vol%), a flow rate of 6 ml/h for the

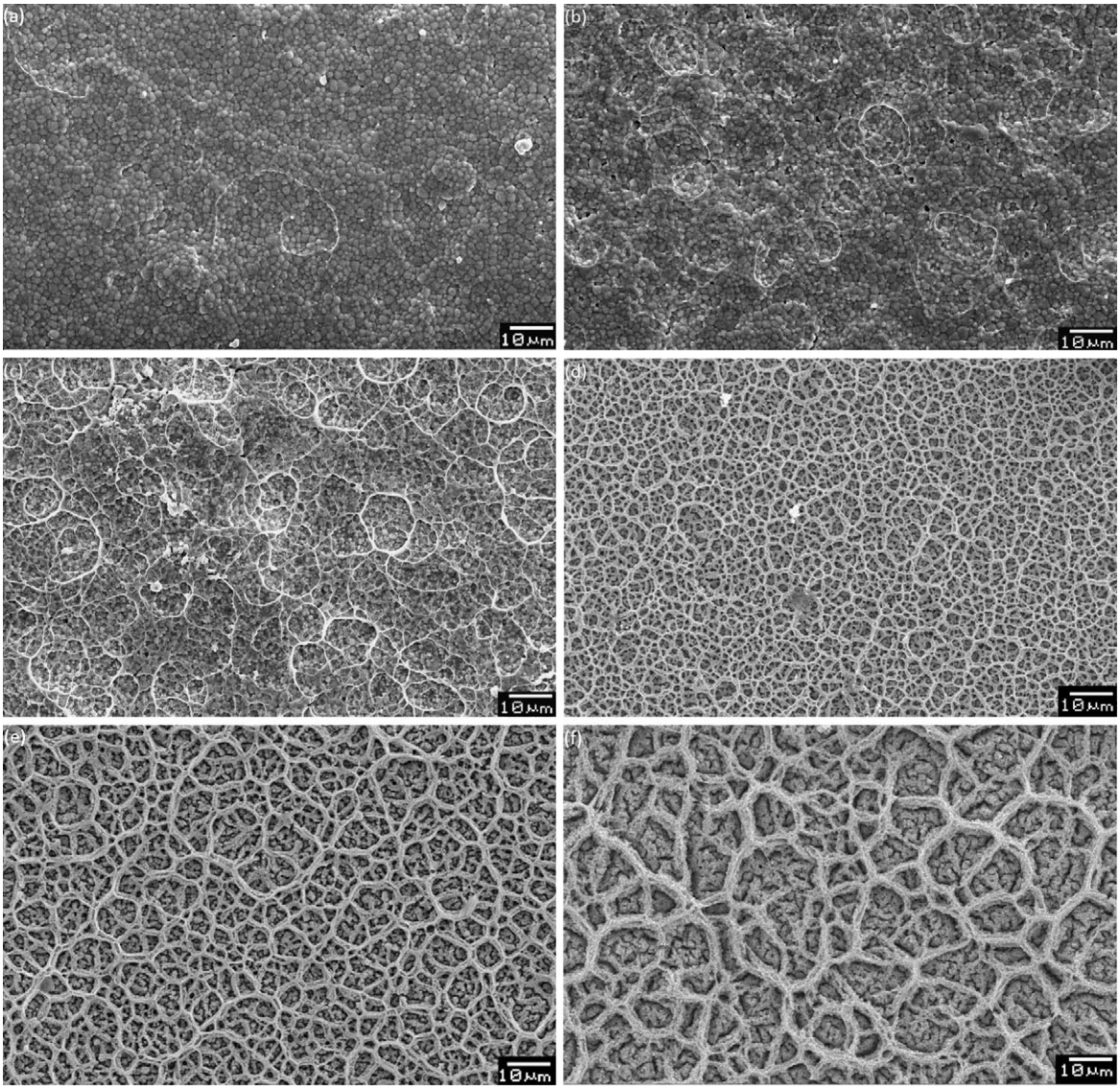

Fig. 9. SEM micrographs of calcined SSC films prepared under 10 kV/3 cm and 350 °C with a deposition time of (a) 1 min, (b) 2 min, (c) 5 min, (d) 10 min, (e) 30 min, and (f) 180 min.

precursor solution, a deposition temperature of 350 °C and an imposed electric field of 10 kV/3 cm.

Symmetrical cells with screen-printed SSC electrodes were also prepared and tested separately for comparison with the cells with reticular electrodes. Typical surface and cross section morphologies of screen-printed SSC electrodes are shown in Fig. 10(a) and (b). The corresponding interfacial ASR values extracted from the impedance spectra, along with that of the reticular SSC electrode and that reported by Lv et al. for another screen-printed SSC electrode[20] and that reported by Xia et al. for a slurry-painted SSC electrode[21] are shown in the Arrhenius plot of Fig. 11 for comparison. ASRs usually decrease with increasing thickness for cathodes of low thicknesses because of the increased reaction sites for oxygen reduction. Beyond a certain thickness, the benefit of increased reaction sites is counterbalanced by the increasing migration length for ions rendering a constant ASR. This was particularly demonstrated in Chang et al.'s work[22] for SSC cathodes where ASR values reached a constant level at a thickness of ~10 μm. While the thickness of current screen-printed electrode was ~100 μm, SSC cathodes of more common thicknesses of 15 μm and 40 μm were obtained respectively by Lv et al.[20] and Xia et al.[21] Therefore, these slurry-based SSC cathodes were thick enough to provide low, constant ASRs. However, these ASRs were still one-half to one order of magnitude larger than that of current ESD electrodes with a thickness close to but smaller than 10 μm. The superior electrochemical performance of the reticular electrode was apparently due to its higher porosity and higher surface area as compared to that of the slurry-based electrodes. Although one may expect a further decrease of ASR using even thicker ESD electrodes, it was not pursued in this work because a further extension of deposition time tended to overgrow the mesh rims and destroy the reticular structure.

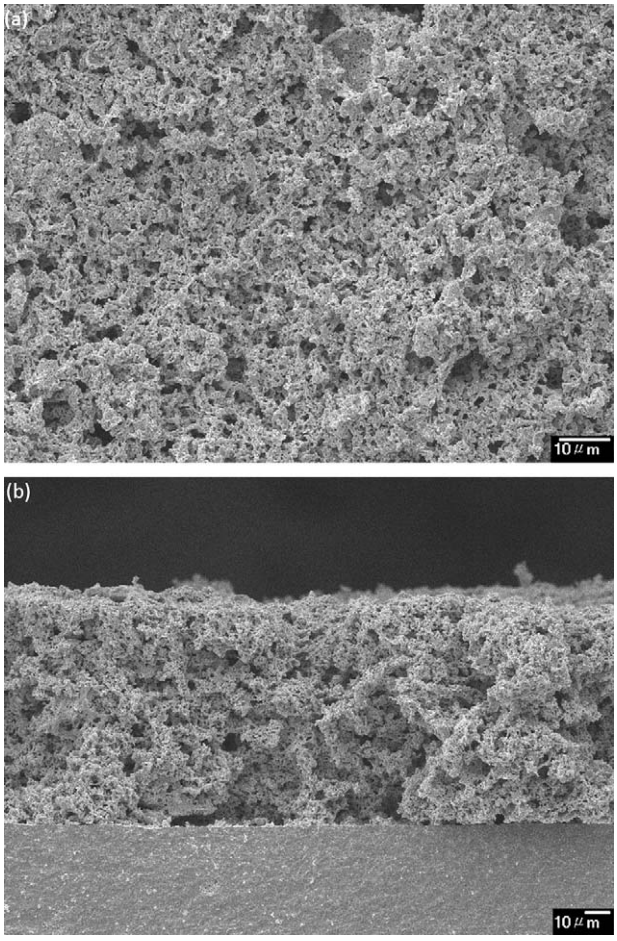

Fig. 10. SEM micrographs showing (a) surface and (b) cross section of a screen-printed SSC electrode.

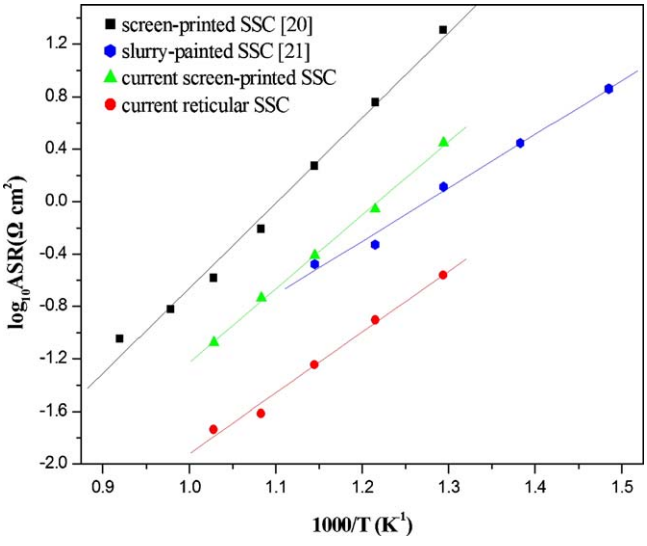

Fig. 11. Arrhenius plots of interfacial ASRs for screen-printed, slurry-painted and reticular SSC electrodes.

4. Conclusion

SSC electrodes with a reticular structure were successfully deposited on CGO substrates by ESD using a set of optimized deposition parameters including a 0.01 M precursor solution containing metal nitrates in a mixture solvent of de-ionized water (0.6 vol%), ethanol (1.5 vol%) and 2-(2-butoxyethoxy)-ethanol butyl carbitol (97.9 vol%), a flow rate of 6 ml/h for the precursor solution, a deposition temperature of 350 °C and an imposed electric field of 10 kV/3 cm. Combination of these optimized deposition parameters rendered aerosol droplets with proper wetness and hence appropriate wetting and spreading on the substrate to form thin layers with isolated holes. Formation of layers of this type is critical for the deposition of a reticular film as the latter is developed by overlapping of these layers.

The inherent high porosity and high surface area in a reticular structure is particularly beneficial for electrochemical performance of SOFC electrodes, and low interfacial ASRs of 0.275, 0.125, 0.057, 0.024 and 0.018 $\Omega\,cm^2$ in the respective operation temperatures of 500, 550, 600, 650 and 700 °C were obtained for current reticular SSC electrodes.

Acknowledgement

Donation of CGO powder by Rhodia (through the help of Brenntag Chemicals in Taiwan) is gratefully acknowledged.

References

1. Matei Ghimbeu C, van Landschoot RC, Schoonman J, Lumbreras M. Tungsten trioxide thin films prepared by electrostatic spray deposition technique. *Thin Solid Films* 2007;**515**:5498–504.
2. Matei Ghimbeu C, Schoonman J, Lumbreras M, Siadat M. Electrostatic spray eposited zinc oxide films for gas sensor applications. *Applied Surface Science* 2007;**253**:7483–9.
3. Matei Ghimbeu C, van Landschoot RC, Schoonman J, Lumbreras M. Preparation and characterization of SnO_2 and Cu-doped SnO_2 thin films using electrostatic spray deposition (ESD). *Journal of the European Ceramic Society* 2007;**27**:207–13.
4. Uchimoto Y, Amezawa K, Furushita T, Wakihara M, Taniguchi I. Charge-transfer reaction rate at the $LiMn_2O_4$ spinel oxide cathode/polymer electrolyte interface. *Solid State Ionics* 2005;**176**:2377–81.
5. Lu J, Chu J, Huang W, Ping Z. Microstructure and electrical properties of $Pb(Zr, Ti)O_3$ thick film prepared by electrostatic spray deposition. *Sensors and Actuators A: Physical* 2003;**108**:2–6.
6. Kim SG, Kim JY, Kim HJ. Deposition of MgO thin films by modified electrostatic spray pyrolysis method. *Thin Solid Films* 2000;**376**:110–4.
7. Chen C, Kelder EM, Paul JJM, van der P, Schoonman J. Morphology control of thin $LiCoO_2$ films fabricated using the electrostatic spray deposition (ESD) technique. *Journal of Materials Chemistry* 1996;**6**:765–71.
8. Marinha D, Rossignol C, Djurado E. Influence of electrospraying parameters on the microstructure of $La_{0.6}Sr_{0.4}Co_{0.2}F_{0.8}O_{3-\delta}$ films for SOFCs. *Journal of Solid State Chemistry* 2009;**182**:1742–8.
9. Jang S, Hwang I, Im J, Park I, Shin D. Fabrication of nickel oxide-yttria stabilized zirconia films by electrostatic spray deposition. *Journal of Ceramic Processing Research* 2009;**10**(6):798–802.
10. Taniguchi I, Hosokawa T. Deposition of SDC and NiO-SDC thin films and their surface, morphology control by electrostatic spray deposition. *Journal of Alloys and Compounds* 2008;**460**:464–71.
11. Hsu CS, Hwang BH, Xie Y, Zhang X. Enhancement of solid oxide fuel cell performance by $La_{0.6}Sr_{0.4}Co_{0.2}Fe_{0.8}O_{3-\delta}$ double layer cathode. *Journal of the Electrochemical Society* 2008;**155**(12):B1240–3.
12. Hwang HB, Chang CL, Hsu CS, Fu CY. Electrostatic spray deposition of NiO/CGO films. *Journal of Physics D: Applied Physics* 2007;**40**(11):3448–55.

13. Fu CY, Chang CL, Hsu CS, Hwang BH. Electrostatic spray deposition of $La_{0.8}Sr_{0.2}Co_{0.2}Fe_{0.8}O_{3-\delta}$ films. *Materials Chemistry and Physics* 2005;**91**:28–35.
14. Taniguchi I, van Landschoot RC, Schoonman J. Fabrication of $La_{1-x}Sr_xCo_{1-y}Fe_yO_3$ thin films by electrostatic spray deposition. *Solid State Ionics* 2003;**156**:1–13.
15. Taniguchi I, Schoonman J. Electrostatic spray deposition of perovskite-type oxides thin films with porous microstructure. *Journal of Materials Synthesis and Processing* 2002;**10**(5):267–75.
16. Princivalle A, Perednis D, Neagu R, Djurado E. Microstructural investigations of nanostructured La(Sr)MnO_3-*ä* films deposited by electrostatic spray deposition. *Chemistry of Materials* 2004;**16**:3733–9.
17. Princivalle A, Perednis D, Neagu R, Djurado E. Porosity control of LSM/YSZ cathode coating deposited by electrospraying. *Chemistry of Materials* 2005;**17**:1220–7.
18. Princivalle A, Djurado E. Nanostructured LSM/YSZ composite cathodes for IT-SOFC: a comprehensive microstructural study by electrostatic spray deposition. *Solid State Ionics* 2008;**179**:1921–8.
19. Nien SH, Hsu CS, Chang CL, Hwang BH. Preparation of $BaZr_{0.1}Ce_{0.7}Y_{0.2}O_{3-\delta}$ based solid oxide fuel cells with anode functional layers by tape casting. *Fuel Cells* 2011;**11**:178–83.
20. Lv H, Wu YJ, Huang B, Zhao BY, Hu KA. Structure and electrochemical properties of $Sm_{0.5}Sr_{0.5}Co_{1-x}Fe_xO_{3-\delta}$ cathodes for solid oxide fuel cells. *Solid State Ionics* 2006;**177**:901–6.
21. Xia C, Rauch W, Chen F, Liu M. $Sm_{0.5}Sr_{0.5}CoO_3$ cathodes for low-temperature SOFCs. *Solid State Ionics* 2002;**149**:11–9.
22. Chang CL, Hsu CS, Hwang BH. Unique porous thick $Sm_{0.5}Sr_{0.5}CoO_3$ solid oxide fuel cell cathode films prepared by spray pyrolysis. *Journal of Power Sources* 2008;**179**:734–8.